

Optimal Scanning, Display, and Segmentation of the International Labor Organization (ILO) X-Ray Images Set for Pneumoconiosis

Marios S. Pattichis¹, Janakiraman Ramachandran¹, Mark Wilson²,
Constantinos S. Pattichis¹ and Peter Soliz²

¹Image and Video Processing and Communication Laboratory (ivPCL)
Dept. of Electrical and Computer Engineering, University of New Mexico, NM, USA
emails: {pattichis, ramanan, costas}@eece.unm.edu
²Kestrel Corporation, Albuquerque, NM, USA
email: mwilson@kestrelcorp.com, zilosp@rt66.com

Abstract

A method for scanning and displaying chest radiographs (x-rays) is presented. The new method treats scanning independent of display, allowing for maximum information content to be captured during the scanning process, and then for this information to be optimally displayed using a new function for maximizing the contrast variation throughout the image. The quality of the digitized x-ray images were compared against the original x-ray films and were found to be of comparable visualization quality. The rib parenchymal is then segmented by an active shape model.

1. Introduction

The chest radiograph is the single most useful tool for clinically evaluating both occupationally related and non-occupational chronic lung diseases. Additionally, it is currently one of the least expensive and the least invasive means by which interstitial lung disease can be detected. Chest radiography is the most important diagnostic test available for screening groups of workers for asymptomatic disease [1].

Examples of x-ray images from the ILO standards database [2] are displayed in Figure 1 (after optimal scanning and display 1(b) and 1(c)). The problem of optimal scanning is viewed as one of maximizing the information content in the scanned image. Because of variations in the radiograph film quality and density, it may not be possible to determine a single scanning procedure that will be quantitatively optimal for all x-ray radiographs. Hence, the challenge is to determine a near optimal procedure based on some quantitative figure-of-merit, then to assess the robustness of the procedure by testing the resulting digital images using trained human observers.

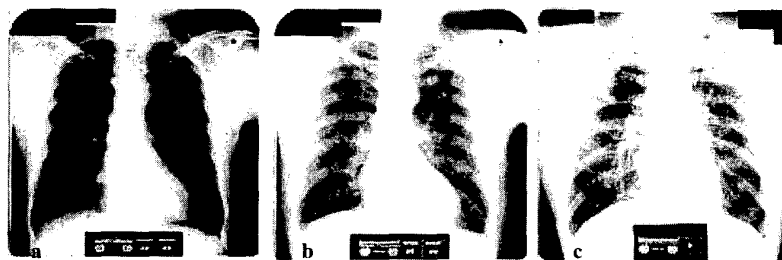


Figure 1. Image scanning and display of the ILO radiographs. In 1(a), the original radiograph of type 2/2 is shown. In 1(b), the same radiograph after logarithmic correction is shown, and in 1(c), a severe case radiograph is displayed (after logarithmic correction).

The image in Figure 1(a) was used to determine the most appropriate exposure for the scanning procedure. This standard image represents a type 2/2 with opacities up to 1.5mm in width [2]. These small opacities are particularly difficult to reproduce on the scanned image. Clearly, the scanning procedures must result in high quality digital images whether applied to a normal non-pathological radiograph, or a severe case as depicted in Figure 1(c). After determining the optimal scanning procedure for the radiograph of Figure 1(a), the same scanning procedure was applied to the entire ILO database.

2. X-Ray Radiograph Scanning and Display

There are three adjustable parameters that were used for scanning on the VXR-12 scanner: (i) the translation table, (ii) the bit depth, and (iii) the exposure level. First, we fixed the bit depth to the maximum possible level of 12 bits per image sample. Then, to help evaluate the scanned image quality, we used: (i) the number of distinct grayscale values in the scanned image, (ii) the minimal and maximal grayscale values to check for possible under-exposure and/or over-exposure, (iii) the entropy over the entire image, and (iv) the entropy over the grayscale values that correspond to the lung region.

The number of distinct grayscale values were used to determine the best exposure level. The maximum number of distinct grayscale values (4096) was obtained for exposure settings between 20 and 40. To determine the optimal exposure setting, we then used the image entropy as a measure of image quality. At a fixed exposure, the entropy is constant regardless of the translation table that is used (for monotone translation tables). Hence, this allowed us to consider the scanning process independent of the display process. The maximum entropy was obtained at an exposure setting of 36 (see Table 1). At this exposure level, the entropy value of 11.38 is near the optimal value of 12. At this exposure level, we scanned the entire ILO set of radiographs, and found that the entropy remained close to the optimal value of 12.

It was found that near-optimal results were also obtained for the rest of the ILO database. Table 2 shows the entropy values for the entire set of 20 standard x-rays.

Table 2. Entropy calculations for each of the 20 ILO standard images, all scanned at an exposure of 36.

Image #	1	2	3	4	5	6	7	8	9	10
Entropy	11.2	11.5	11.6	11.2	11.6	11.6	11.5	11.6	11.4	11.4
Image #	11	12	13	14	15	16	17	18	19	20
Entropy	11.4	10.9	11.3	11.3	11.4	11.5	11.3	11.8	11.5	11.4

To determine the optimal display parameters, we defined a translation function $I_n(i, j) = \log_{10}(1 + 10^n I(i, j))$ where n needs to be determined for optimal visual perception of the displayed image. In order to determine n , we introduce an optimization function $g(I_n(i, j))$ that should be maximum for the optimal value of n . For g , a new function was considered that captures variations in the perceived image contrast that is computed as the sum of the contrast

Table 1. Exposure vs. Entropy results. Maximum entropy is at exposure=36. The frequency count at the maximum grayscale value was not used for the entropy.

Exposure	Entropy
10	9.74
12	9.95
15	10.24
18	10.49
20	10.61
22	10.74
24	10.84
25	10.88
28	11.04
30	11.13
32	11.22
34	11.29
35	11.34
36	11.38
37	11.37
38	11.36
40	11.32

variations along the columns and rows. The value of $n=3$ was found to be near optimal in all cases.

3. Digital Image Quality Assessment

To assess the quality of the digitized x-ray images, we performed an image quality assessment test. The test consisted of assigning an absolute rating to each mode for 7 grading criteria. Mode 1 was defined as the original film, while mode 2 was the digital x-ray image. The criteria used to evaluate the two modes were the following:

Anatomical Structures:

- A. Visualization of vessels approximately 3cm from pleural margin.
- B. Visualization of vessels *en face* in central area.
- C. Visualization of the Carina with main bronchi.
- D. Visualization of thoracic vertebrae behind heart.
- E. Visualization of pleural margin.

Opacities:

- F. Visualization of opacities in the most affected region.
- G. Visualization of opacities in the least affected region.

The absolute scale used was: 1=Not visible, 2=Poorly visualized, 3=Adequately visualized, 4=Very well visualized. The average of the differences between the two modes (mode 1 – mode 2) are given in Table 3 for the 7 criteria. The results are also plotted to help visual interpretation. The maximum value for any criterion would be 3, which would mean one mode was very well visualized while the other was not visible for every x-ray. All of the values are positive meaning that the original x-ray films were preferred for all 25 x-rays with exception of B where the digital image and x-ray films are equally visualized. Criteria C and D showed a high preference for mode 1 with almost a point difference, while A, B, and G show very little preference for the original x-ray film. The E and F criteria are low as well with an average difference of 0.36 and 0.28 points on average. This gave a measure of the relative preference for a single mode showing C and D are preferred in mode 1 (x-ray film) by more than half a point and almost a point respectively. Taking this into consideration one would also like to know the average criteria values for each mode in order to judge the magnitude of the visualization preference. The average visualization values by criterion for the two modes are in Table 4 and Figure 2.

Table 3. Average of differences between modes 1 and 2 for each criterion.

Criteria	A	B	C	D	E	F	G
	0.08	0	0.68	0.84	0.36	0.28	0.08

Table 4. Average visualization values for modes 1 and 2, and for each criterion.

Criteria	A	B	C	D	E	F	G
Mode 1	3.12	3.8	2.88	2.76	3.76	3.8	3.44
Mode 2	3.04	3.8	2.2	1.92	3.4	3.52	3.36

These values show criterion A was adequately visualized for both modes. Criterion B is close to being very well visualized for both modes. In criterion C mode 1 is close to being adequately visualized while mode 2 is closer to poorly visualized. The D criterion was close to being adequately visualized in mode 1 but just under poorly visualized for mode 2. This shows a large difference in preference for this particular criterion, favoring mode 1. In mode 1 criteria E and F was close to being very well visualized while mode 2 is between adequately and very

well. Criterion G for both modes is just above adequately, yet there is little difference between the two.

With these two pieces of information the magnitude of the differences is shown and the overall rating for these criteria is shown. Clearly criteria C and D were favored in mode 1 while still only being on average close to adequately visualized. The E and F were slightly preferred over mode 2 yet both modes have average values above adequately visualized. The G was also very slightly preferred in mode 1 yet the average magnitudes for each are above adequate. For A again mode 1 was slightly preferred while both had average values above adequate. The dead heat was criteria B which showed no mode preference but had a high rating just below very well visualized.

Using a one-tailed t test with a 97.5% confidence interval the following null and alternative hypotheses were tested, $H_0: \mu_1 - \mu_2 = 0$ $H_1: \mu_1 - \mu_2 > 0$ for each criteria, where 1 represents mode 1 and 2 is mode 2. The rejection region for this test is, $t \geq 2.021$ and the obtained probability level of the result is $p < 0.0005$. The resulting t values are in Table 5. The t value was in the rejection region for criteria C, D, E, and F therefore rejecting H_0 in favor of H_1 . Criteria A, B, and G were not in the rejection region, therefore there is not a significant difference between mode1 and mode2 for these criteria.

Table 5. t test values for each criteria.

Criteria	A	B	C	D	E	F	G
t values	0.3196	0	2.7517	3.861	2.1669	2.1433	0.4007

4. Rib Segmentation

Segmentation was performed using an adaptive shape model (ASM) [3]. Starting with 10 ILO standard images, a shape model was constructed for four separate lung regions, i.e. upper and lower, right and left combinations. Dividing the lung in such a manner improved convergence. The parenchyma (region between the ribs) was segmented. It is the parenchymal regions that provide the best view of the opacities related to pneumoconiosis.

An example of a segmentation for the upper right lung is given in Figure 3. In this image only the posterior rib parenchyma were segmented.

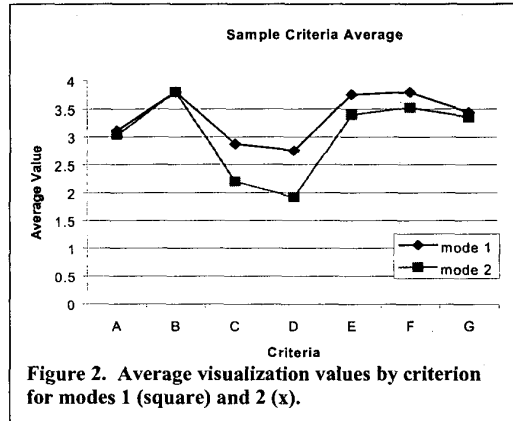


Figure 2. Average visualization values by criterion for modes 1 (square) and 2 (x).

5. Conclusion and Ongoing Work

A new system for optimal scanning, display and segmentation of the ILO chest radiograph set has been presented. The segmented regions will be used in developing a fully automated system for classifying radiographs into the different types of pneumoconiosis. The success of the ASM in segmenting the parenchymal region is due partly to the judicious application of optimal parameters. The image quality tests showed that the digital images were indeed of sufficient quality to allow the pulmonologists to accurately diagnose the digital radiographs.

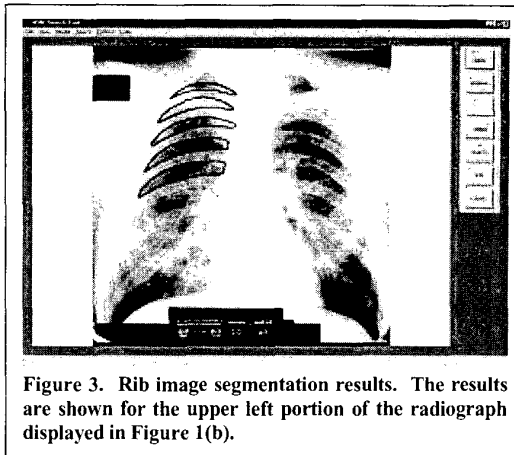


Figure 3. Rib image segmentation results. The results are shown for the upper left portion of the radiograph displayed in Figure 1(b).

6. Acknowledgements

Funding for the study was through a grant from the National Institute for Occupational Safety and Health (NIOSH), Grant 2R44 OHRRGM 03595. The chest radiograph data were provided by Miners' Colfax Medical Center (MCMC) Outreach Program. We gratefully acknowledge Dr. David James, M.D., and Dr. L. Ketai, M.D., from the University of New Mexico Health Sciences Center, Albuquerque, New Mexico.

7. References

1. Ridlich, C.A., *Pulmonary fibrosis and interstitial lung diseases*, in *Occupational and Environmental Respiratory Disease*, P. Harber, M.B. Schenker, and J.R. Balmes, Editors. 1996, Mosby-Year Book, Inc.: St Louis, MO, p. 2116-227.
2. *Guidelines for the use of ILO international classification of radiographs of pneumoconioses*, 1980, International Labour Office: Geneva.
3. Cootes, T.F., C. J. T. Taylor, D. H. Cooper and J. Graham. *The Use of Active Shape Models for Locating Structures in Medical Images*, *Image and Vision Computing*, July 1994, 12(6): p. 355-356.